WHERRETT LABORATORY OF NUCLEAR CHEMISTRY

Department of Chemistry

University of Pittsburgh
15260

NUCLEAR CHEMISTRY RESEARCH

Principal Investigator

Robert L. Wolke

Professor of Chemistry

ANNUAL PROGRESS REPORT

1 January - 31 December 1975

U.S.E.R.D.A. Contract E(11-1)3427

Report Number COO-3427-14

DISCLAIMER

TABLE OF CONTENTS

I. INTRODUCTION

Calendar 1975 saw the initiation of a major new research project at the Van de Graaff, in collaboration with Nuclear Physics Laboratory personnel. (See A, Heavy-Ion Fusion Reactions, below.) In addition, the equilibrium charge-state distribution project at the Van de Graaff has progressed to the completion of data taking and the beginning of the analysis of shell effects (section B, below).

Among our studies not involving the Van de Graaff, the generalized statistical examination of low-level counting data has been completed and submitted for publication (section C, below), while the measurements of total strontium and radiostrontium in marine molluscan shells has progressed through the development of reliable analytical and radioanalytical procedures, so that routinized analyses of many specimens can be made (section D, below).

Also described in this report (sections E and F) are the substantial improvements in radioactivity counting, target preparation, and Van de Graaff source facilities which were accomplished during 1975. Finally, (section G), a brief summary is given of the extensive computer usage by our group during the year.

All the new equipment described in sections E and F was obtained with non-ERDA funds: from the Pennsylvania Dept. of Property and

Supplies' fund for equipping the Chemistry Department's new building. All of the computation described in section G was paid for by the University out of the indirect costs associated with its research contracts.

II. SUMMARY OF RESEARCH

A. Heavy-Ion Fusion Reactions

During the past year, a heavy-ion induced complete fusion experiment was initiated. This project involves the formation of the compound nucleus ^{50}Cr through the following five entrance channels:

Target	Projectile
^{26}Mg	^{24}Mg
^{27}Al	^{23}Na
^{31}P	^{19}F
^{32}S	^{18}O
^{35}Cl	^{15}N

Bombardment energies range from 20% below the coulomb barrier to the highest energy attainable with the three-stage tandem Van de Graaff. The effect of the entrance channel on the limiting angular momentum, ℓ_{crit}, which characterizes the fusion process, is being investigated.

Table A1 shows the five systems under study in this experiment, along with some important parameters for each system. In the example of Table A1, the incident energies of all the projectiles were chosen to give the ^{50}Cr compound nucleus an excitation energy of 45 MeV. The excitation energy of all five systems will overlap within the energy range to be studied. Also, the grazing angular momenta are very nearly equal. Identical compound nuclei should therefore be

TABLE A1 Target-projectile systems utilized in complete fusion reaction studies.

TARGET	PROJECTILE	V_c(MeV)	Q(MeV)	E^*(MeV)	E_{cm}(MeV)	$\ell_{grazing}$($\hbar$)	ℓ_{Bass}($\hbar$)
^{26}Mg 0	^{24}Mg 0	22.2	20.1	45.0	24.9	32.2	24.2
^{35}Cl 3/2	^{15}N 1/2	18.7	21.3	45.0	23.7	28.3	23.0
^{32}S 0	^{18}O 0	19.9	23.5	45.0	21.5	28.5	22.8
^{31}P 1/2	^{19}F 1/2	20.9	24.3	45.0	20.7	28.3	22.0
^{27}Al 5/2	^{23}Na 3/2	22.0	23.5	45.0	21.5	29.8	22.5

formed from all five entrance channels, permitting one to isolate any effects due to the entrance channel. In each case, the limiting angular momenta ℓ_{Bass} calculated from the Bass model [Nucl. Phys. A216, 386 (1974)] are significantly lower than $\ell_{grazing}$. This experiment should therefore be the first test of the Bass model in this energy region. If the Bass model is obeyed by the systems being considered, the ℓ_{crit} values will differ by only two units of angular momentum. Detection of this small difference is expected to be difficult, but not impossible. (For further details of the rationale and purposes of these experiments and of the experimental arrangement, see the accompanying Proposal for Continuation.)

Thus far, two successful preliminary runs have been performed on this experiment. The first of these runs was a shake-down run, in which the reaction of ^{16}O on ^{27}Al was observed. This particular target-projectile combination was chosen because experiments involving direct reactions on this system had already been performed at the Nuclear Physics Lab. It was felt that this system would provide a severe test of the detection system, the electronics, the data acquisition program and the data analysis program. (Details of these can be found in the accompanying Proposal for Continuation.) During this run a few problems were discovered, some of which were solved by minor modifications in the experimental setup while others required hardware modifications of the ADC. It is currently felt that all of the problems discovered during the initial shake-down run have been satisfactorily solved, and extensive testing since this run has revealed no new problems.

The second run was devoted to the development of a ^{24}Mg beam.

In preparation for this run, a MgO cone was fabricated and installed in the UNIS source. The output from this cone was mass-analyzed by a 20° inflection magnet prior to injection into the Van de Graaff. At this point, 600 na of MgO^- were observed. After acceleration, however, only 0.016 na of Mg^{7+} could be tuned into the scattering chamber. This was a large enough amount of beam to verify that magnesium was being accelerated, but not enough to attempt a nuclear reaction experiment.

The extensive computer work which has been done in connection with this experiment is summarized in Section G, below. Further runs have been scheduled and the experiment is to continue in accordance with the accompanying Proposal.

B. Equilibrium Charge-State Distributions of Heavy Ions

During the past year, equilibrium charge-state distributions have been measured for accelerator-produced ^{58}Ni and ^{48}Ti ions. The distributions were measured at 0° for ions passing through 20 μg/cm² self-supporting carbon foils at a series of energies ranging from 9 to 72 MeV. The experimental arrangement was the same as has been described previously (COO-3427-10).

The measured charge-state distributions of ^{58}Ni ions are shown in Table B1 and are plotted as a function of energy in Figure B1. The analogous data for ^{48}Ti ions are shown in Table B2 and are plotted in Figure B2. The mean charge $\overline{Q}$, the distribution width d, and the skewness of the distributions are also included in the tables.

As expected, the mean charge of both ions increases with increasing energy, the ^{58}Ni distributions exhibiting a mean charge higher than the ^{48}Ti distributions at the same energies.

The horizontal spacings between the curves of Figs B1 and B2 may be thought of as corresponding to the added energy required to remove a given electron from the ion after the previous electron has been removed. Figure B1 shows that for ^{58}Ni ions, the spacings between the positively sloping parts of the curves are approximately constant until the charge 18+ is reached, at which point the spacing increases dramatically. The 18+ → 19+ transformation corresponds to the crossing of the M-L shell juncture. When the charge state 18+ has been achieved, the M shell has been completely emptied; in order to reach higher charge-states, electrons must be removed from the L shell. Since L-shell electrons are more tightly bound than M-shell electrons, more energy must be expended to remove them from the ion. The energy spacings within a given shell, however, appear

Table B1: Equilibrium charge-state data for ^{58}Ni ions. Column headings are identified below the table.

E	QB	D	S	8+	9+	10+	11+	12+	13+	14+	15+	16+	17+	18+	19+	20+	21+	22+	23+
15.00	12.69	1.48	.124	0.12	0.93	5.00	14.77	25.39	25.18	17.21	8.24	2.62	0.54	*****	*****	*****	*****	*****	*****
			+/-	0.01	0.01	0.02	0.06	0.11	0.12	0.08	0.05	0.02	0.01	*****	*****	*****	*****	*****	*****
21.00	13.00	1.51	.128	0.06	0.55	3.41	11.44	22.54	25.84	20.16	10.91	3.98	0.97	0.15	*****	*****	*****	*****	*****
			+/-	0.01	0.01	0.03	0.13	0.27	0.31	0.24	0.13	0.05	0.01	0.01	*****	*****	*****	*****	*****
30.00	14.52	1.62	-.023	*****	0.04	0.38	2.31	7.85	16.22	22.60	22.84	16.45	8.29	2.80	0.21	0.01	*****	*****	*****
			+/-	*****	0.01	0.01	0.01	0.06	0.12	0.20	0.20	0.14	0.08	0.02	0.01	0.01	*****	*****	*****
40.00	15.77	1.61	-.251	*****	*****	0.05	0.40	2.00	6.24	12.96	20.27	23.55	19.89	12.22	2.16	0.25	0.02	*****	*****
			+/-	*****	*****	0.01	0.01	0.02	0.07	0.14	0.22	0.25	0.22	0.13	0.02	0.01	0.01	*****	*****
45.00	16.20	1.59	-.318	*****	*****	0.01	0.18	1.13	3.97	9.60	16.99	22.78	22.92	17.60	4.14	0.62	0.05	*****	*****
			+/-	*****	*****	0.01	0.01	0.01	0.02	0.04	0.06	0.08	0.07	0.06	0.01	0.01	0.01	*****	*****
50.00	16.77	1.53	-.430	*****	*****	*****	0.07	0.46	1.91	5.58	12.00	19.75	24.80	25.04	8.50	1.87	0.01	*****	*****
			+/-	*****	*****	*****	0.01	0.01	0.01	0.02	0.05	0.08	0.08	0.08	0.02	0.01	0.01	*****	*****
55.00	17.11	1.48	-.425	*****	*****	*****	*****	0.24	1.16	3.76	9.12	16.92	24.59	29.22	11.67	2.90	0.42	*****	*****
			+/-	*****	*****	*****	*****	0.01	0.01	0.02	0.06	0.11	0.16	0.18	0.07	0.01	0.01	*****	*****
60.00	17.43	1.45	-.432	*****	*****	*****	*****	0.13	0.69	2.49	6.68	13.88	22.92	31.72	15.84	4.81	0.86	*****	*****
			+/-	*****	*****	*****	*****	0.01	0.01	0.02	0.04	0.07	0.11	0.14	0.07	0.01	0.01	*****	*****
66.00	17.85	1.40	-.333	*****	*****	*****	*****	*****	0.31	1.30	4.09	10.11	19.78	33.24	20.99	8.13	1.82	0.23	*****
			+/-	*****	*****	*****	*****	*****	0.01	0.01	0.03	0.06	0.11	0.18	0.11	0.03	0.01	0.01	*****
72.00	18.47	1.35	-.190	*****	*****	*****	*****	*****	0.06	0.36	1.68	5.00	13.31	30.63	27.87	15.12	4.97	0.91	0.08
			+/-	*****	*****	*****	*****	*****	0.01	0.01	0.01	0.03	0.07	0.16	0.15	0.08	0.02	0.01	0.01

Column heading symbols: E = ion energy in MeV, QB = mean charge, D = width of the distribution, S = skewness of the distribution. Errors are listed directly under the charge fractions.

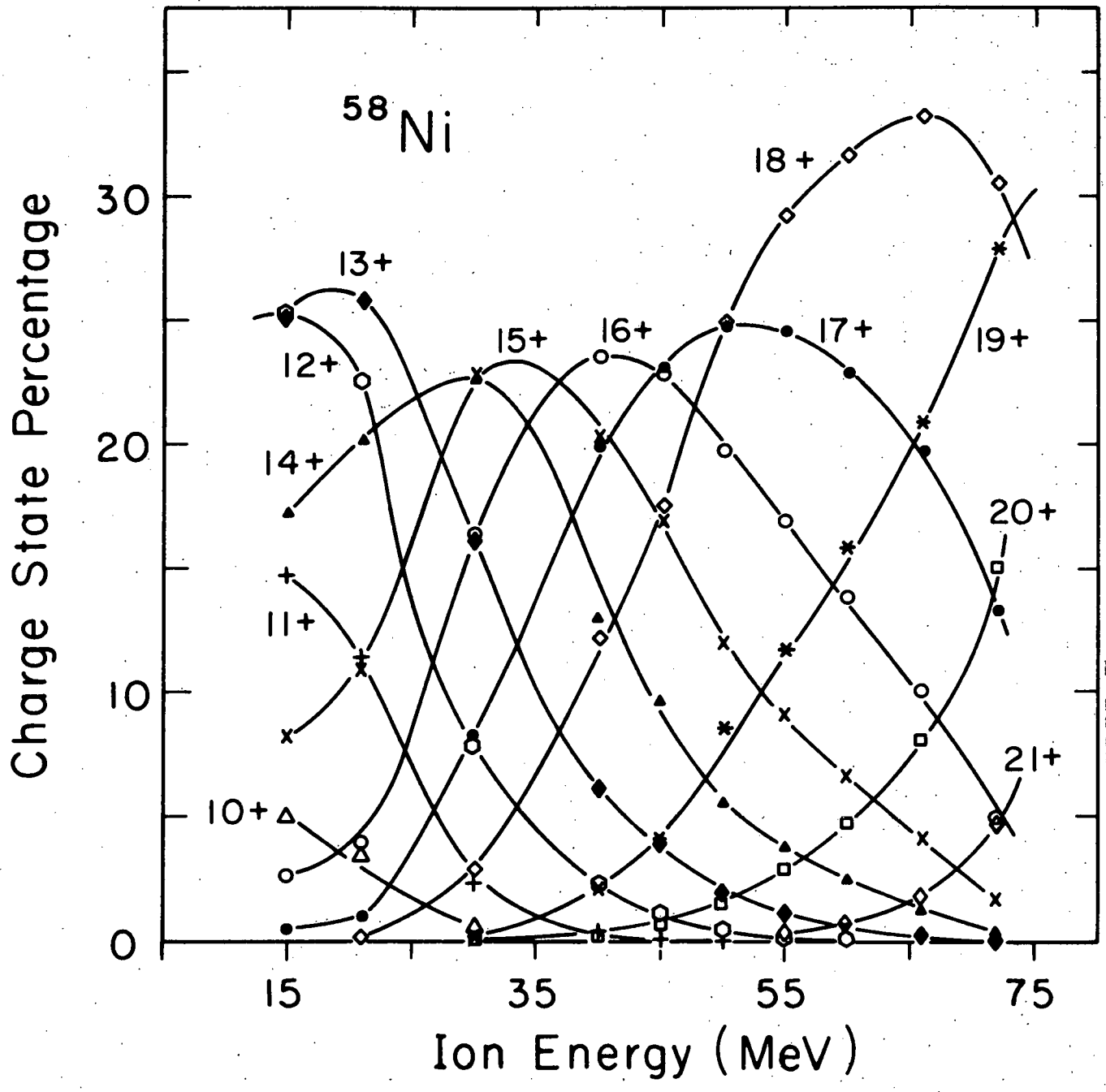

Figure B1: Charge-state abundances of ^{58}Ni ions equilibrated in a carbon foil.

Table B2: Equilibrium charge-state data for ^{48}Ti ions. Column headings are listed below the table.

E	QB	D	S	5+	6+	7+	8+	9+	10+	11+	12+	13+	14+	15+	16+	17+	18+	19+
9,00	6,25	1,53	-,070	0,42	2,91	9,90	18,67	23,96	22,22	15,02	6,21	0,68	*****	*****	*****	*****	*****	*****
			+/-	0,01	0,01	0,04	0,07	0,09	0,10	0,07	0,03	0,01	*****	*****	*****	*****	*****	*****
12,00	10,34	1,48	-,310	0,04	0,48	2,89	8,15	16,30	23,28	25,13	18,95	4,26	0,48	0,03	*****	*****	*****	*****
			+/-	0,01	0,01	0,02	0,05	0,09	0,12	0,12	0,08	0,01	0,01	0,01	*****	*****	*****	*****
20,00	11,90	1,28	-,225	*****	*****	*****	0,59	3,31	9,44	20,84	34,56	22,16	7,66	1,34	0,11	*****	*****	*****
			+/-	*****	*****	*****	0,01	0,01	0,03	0,08	0,16	0,11	0,04	0,01	0,01	*****	*****	*****
32,00	13,10	1,28	-,103	*****	*****	*****	0,05	0,40	1,76	6,91	22,09	31,35	24,47	10,43	2,31	0,23	*****	*****
			+/-	*****	*****	*****	0,01	0,01	0,01	0,03	0,10	0,15	0,13	0,06	0,01	0,01	*****	*****
40,00	13,67	1,26	,021	*****	*****	*****	*****	0,08	0,51	2,74	14,18	27,61	29,95	17,91	5,69	1,10	0,04	*****
			+/-	*****	*****	*****	*****	0,01	0,01	0,01	0,07	0,14	0,17	0,11	0,04	0,01	0,01	*****
46,50	13,97	1,29	-,003	*****	*****	*****	*****	*****	0,32	1,90	10,02	23,32	30,63	22,39	9,29	1,97	0,17	*****
			+/-	*****	*****	*****	*****	*****	0,01	0,01	0,06	0,14	0,16	0,10	0,03	0,01	0,01	*****
54,00	14,41	1,28	-,010	*****	*****	*****	*****	*****	*****	0,85	5,67	17,04	29,02	27,65	15,06	4,22	0,48	0,02
			+/-	*****	*****	*****	*****	*****	*****	0,01	0,03	0,10	0,16	0,14	0,07	0,02	0,01	0,01
60,00	15,29	1,29	-,295	*****	*****	*****	*****	*****	*****	0,21	1,70	6,79	17,47	27,78	28,66	14,93	2,46	0,02
			+/-	*****	*****	*****	*****	*****	*****	0,01	0,01	0,02	0,07	0,12	0,14	0,08	0,03	0,01

Column headings symbols: E = ion energy in MeV, QB = mean charge, D = width of the distribution, S = skewness of the distribution. Errors are listed directly under the charge fractions.

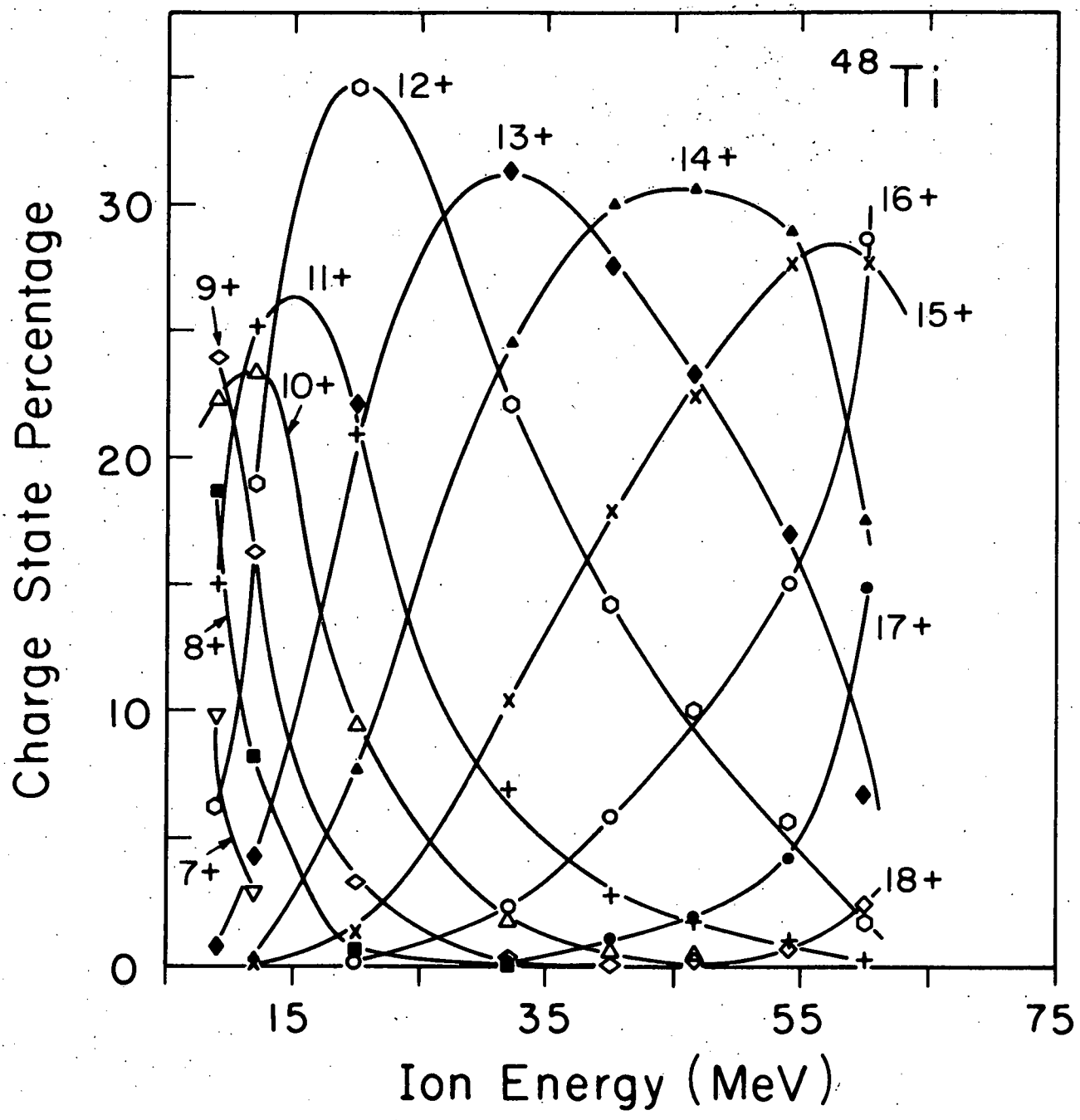

Figure B2: Charge-state abundances of ^{48}Ti ions equilibrated in a carbon foil.

to be constant.

The maximum heights of the charge-state curves of Fig. B1 are seen to increase as nickel's M shell is emptied, the 18+ peak being considerably higher than the lower charge-state curves. This can be understood in terms of competition, the removal of the nineteenth electron (the first L electron) being suppressed by the larger energies required for the removal of L electrons, leading to an enhancement of the 18+ abundance.

Figure B2 is a plot of charge fraction vs. energy for ^{48}Ti ions equilibrated in carbon. In this figure, the spacings between the positively-sloping portions of the curves increase between 12+ and 13+. In titanium, the 12+ ion has a completely emptied M shell; removal of the first L shell electron is required to achieve a charge-state of 13+. As in the nickel data, the peak of the curve corresponding to the emptied ^{48}Ti M shell is higher than for the lower charge-state curves.

Although charge-state distributions are generally assumed to be gaussian, there are a number of factors that may cause deviations from the gaussian shape. Among these are density effects and multiple electron loss during single collisions. Deviations in certain energy regions may also be ascribed to the electronic structure of the ions: if some electrons are unusually difficult to remove, for example, the result will be a skewed distribution.

A semilog plot of the ratio F(Q+1)/F(Q) against Q, where Q is the ionic charge state and F(Q) is the charge fraction of state Q, should be linear for a pure gaussian distribution. Deviations from gaussian shape tend to affect the linearity of such a plot quite sensitively. Figure B3 shows the ^{58}Ni data plotted in this way. The curves are all reasonably linear at low charge states, but a sharp break occurs at every energy at F(19)/F(18), the position of the M-L shell juncture.

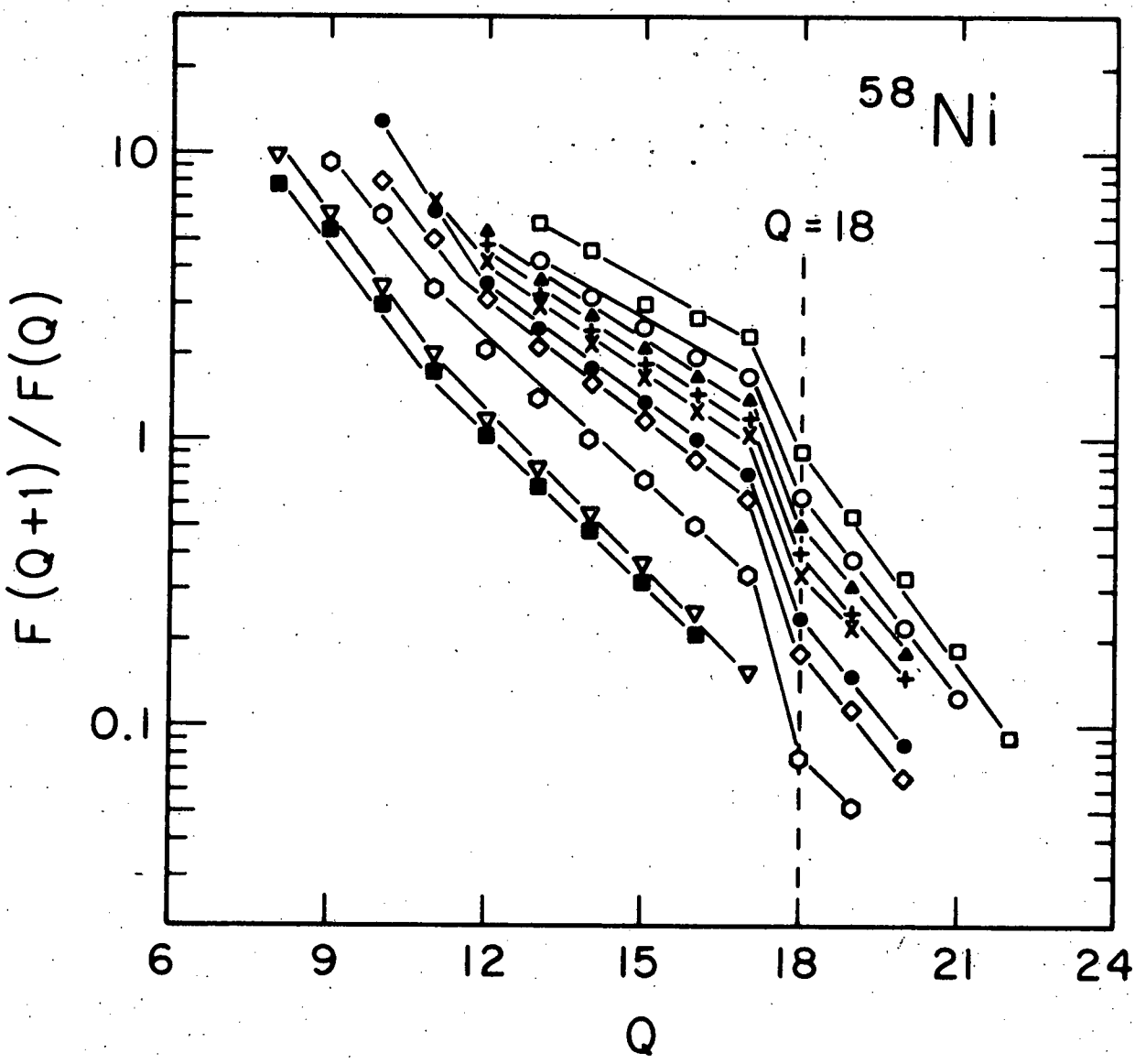

Figure B3: Charge fraction ratio discontinuities due to shell effects in ^{58}Ni ions. The energies of the curves in MeV, reading from top to bottom are: 72, 66, 60, 55, 50, 45, 40, 30, 21.

Figure B4 is a plot of F(Q+1)/F(Q) vs Q for titanium ions. In this case there is a break at Q = 12, (F(13)/F(12)) corresponding to the M-L shell juncture in titanium. Another break in the curves seems to be present at Q = 17, which does not correspond to any obvious feature of electronic structure and is yet to be explained.

After a beam of ions has achieved charge-state equilibrium, the charge-increasing processes and the charge-decreasing processes are balanced for each charge. This condition may be expressed as

$$\frac{\sigma_{Q(\text{loss})}}{\sigma_{Q(\text{capture})}} = \frac{F(Q)}{F(Q-1)}$$

where σ is the electron capture or loss cross section. Thus the ratio of the probability of loss of electron Q to the probability of its capture is equal to the ratio of the charge fractions. When the ratio equals unity, the capture and loss probabilities for electron Q are equal and the electron may be said to be in equisection.

Figure B5 shows the charge-fraction F(Q)/F(Q-1) as a function of ion velocity for ^{58}Ni ions. Comparing the velocity spacings between the lines at a constant charge-fraction ratio, particularly at the equisection velocity at which F(Q)/F(Q-1) = 1, one can see that the lines are separated by an approximately constant velocity for electrons within each shell, but that between the F(18)/F(17) and the F(19)/F(18) lines, the velocity spacing is much bigger. If these spacings can be interpreted

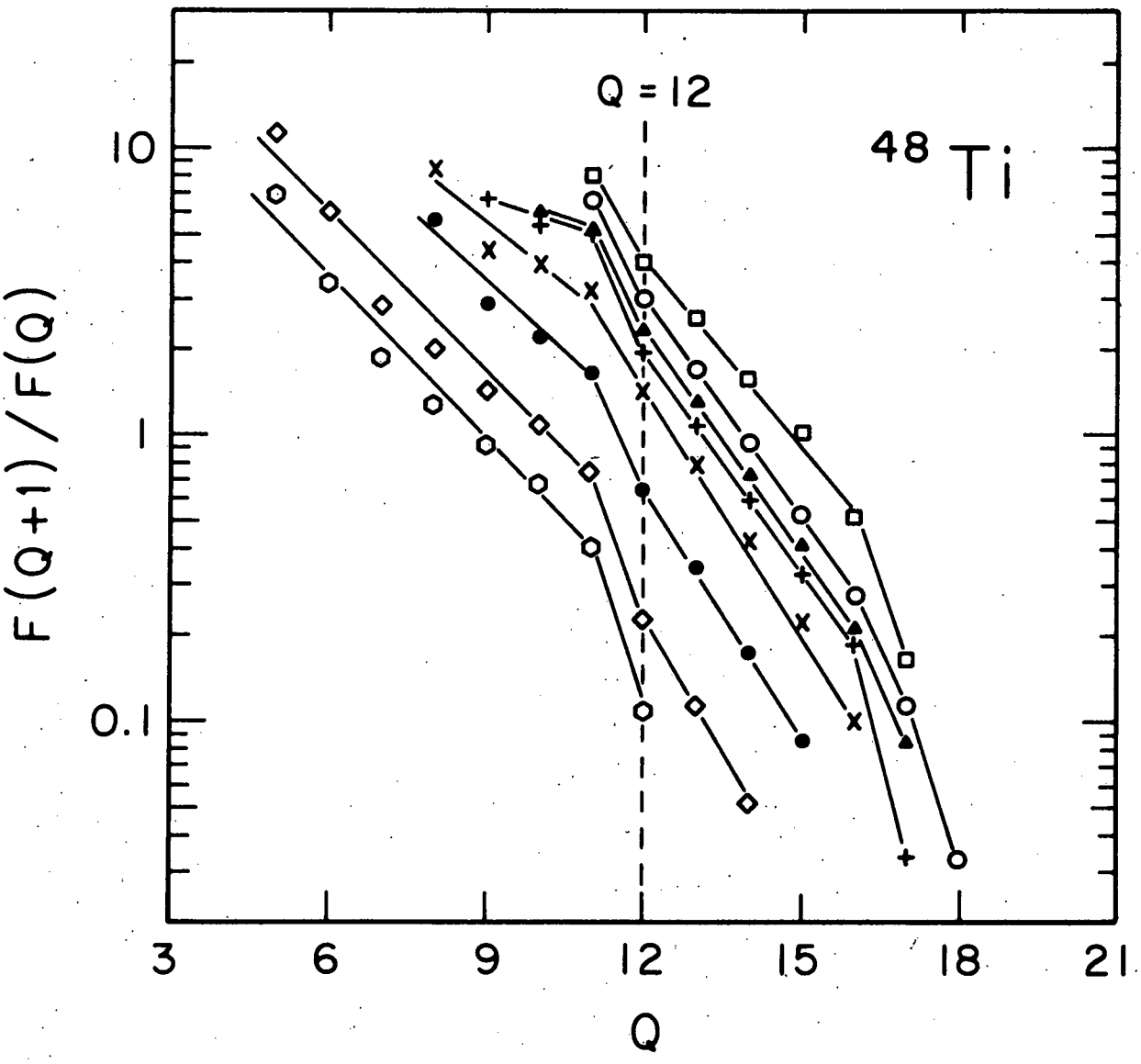

Figure B4: Charge fraction ratio discontinuities due to shell effects in ^{48}Ti ions. The energies of the curves in MeV, reading from top to bottom are: 60, 54, 46.5, 40, 32, 20, 12, 9.

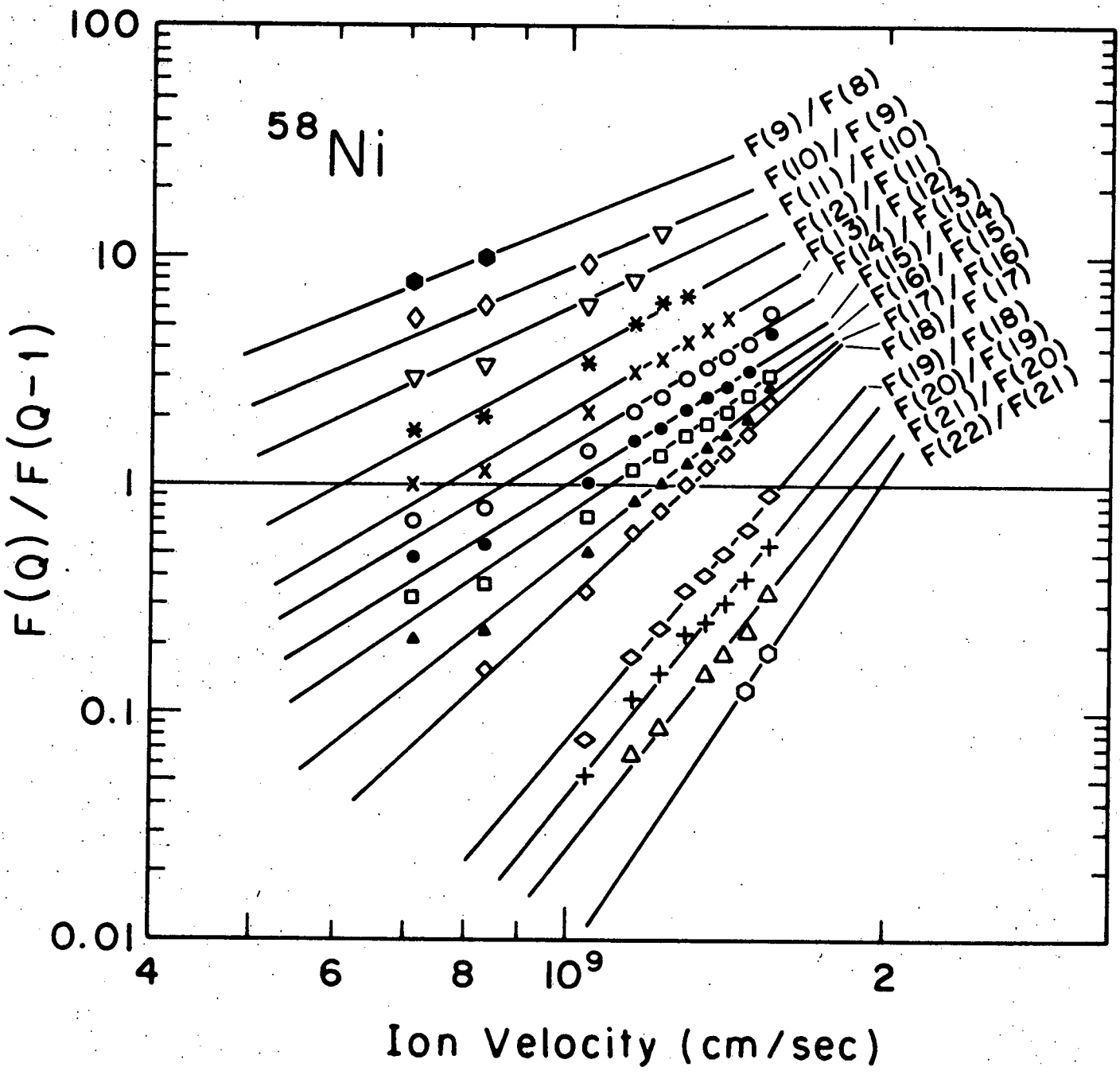

Figure B5: Charge fraction ratios of ^{58}Ni ions as a function of velocity.

as the additional ion velocity required for an electron to achieve a given loss-to-capture ratio (for example, unity) after the preceding electron has done so, we again see the L-M energy separation reflected clearly in the charge-state behavior of the ions.

Figure B6 is the ^{48}Ti data plotted as F(Q)/F(Q-1) *vs* velocity. The same spacing increase between shells may be seen here as in the ^{58}Ni data. The large spacing in ^{48}Ti occurs between the F(12)/F(11) and F(13)/F(12) lines, again corresponding to the L-M shell boundary.

Although these data show only gross effects of shell structure on charge-state distributions, there is evidence in the data of possible finer, or sub-shell effects. These are currently under investigation. Moreover, it appears that the lines in Figs. B5 and B6 may converge to a point or points at some high velocity or velocities. The data are currently being analyzed statistically to determine if such convergence points actually exist. If so, a knowledge only of the convergence points, the velocity separations at equisection, and one charge-state distribution would suffice to reproduce the complete equilibrium charge-state distributions of one or more heavy ions at any energy. This would, of course, be an extremely powerful tool for workers in heavy-ion acceleration technology. Attempts are therefore under way in our laboratory to seek theoretical justification for the existence of convergence points in charge-fraction-ratio *vs* velocity plots and, if possible, to predict the convergence points for the various electronic shells.

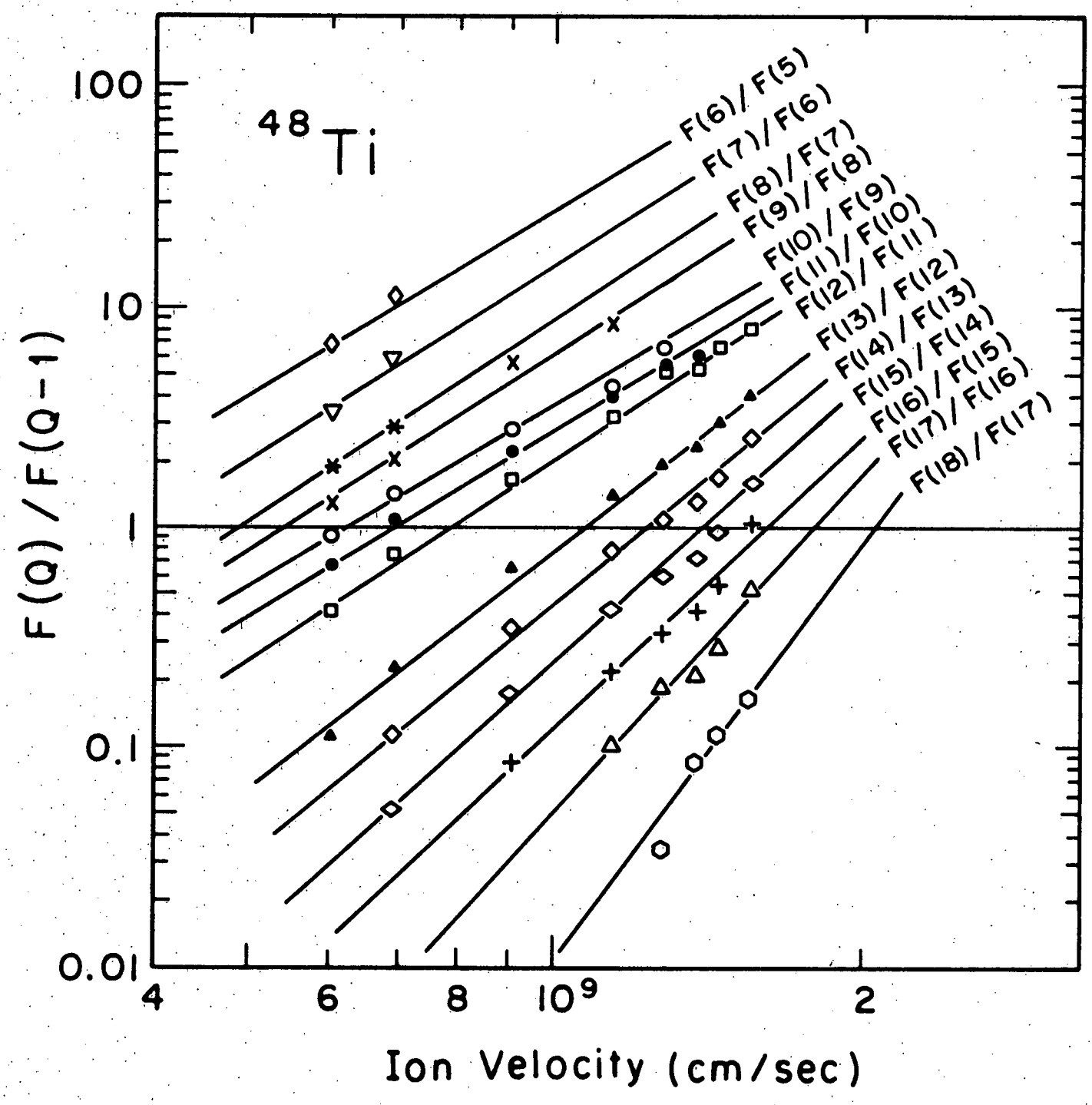

Figure B6: Charge fraction ratios of ^{48}Ti ions as a function of velocity.

C. The statistics of Low-Level Counting

A statistical examination of low-level, or background-dominant, counting of radioactivity, reported upon briefly in last year's report (COO-3427-10), has been completed. The objective of this work was to provide a consistent, statistically defensible, practical guide for counting technicians in the field of monitoring very low levels of activity.

The role of very low levels of radioactivity in physical and ecological systems is attracting an increasing amount of attention as nuclear power increases in importance throughout the world. Any conclusion which may be drawn regarding the importance of very low levels of radioactivity in the environment, however, must ultimately be based upon quantitative counting measurements on samples, the gross activities of which may be very close to background or to the activity of a blank sample. In such background-dominant situations, both the design of the counting experiment and the interpretation of the data must follow statistically defensible procedures if the conclusions are to be meaningful.

Two questions are of primary practical importance: "Does the sample exhibit a net activity above background?" and "Is the sample's activity below some predetermined acceptable limit?" The first of these questions is of importance in studies of very long-lived, naturally-occurring radionuclides, while the second can be of vital concern in environmental monitoring. Statistically valid prescriptions for the optimal design and interpretation of a counting experiment to answer these two questions do not appear to exist explicitly, using consistent formalism, in any single location in the literature.

In a previous treatment of the first question, "Does the sample exhibit a net activity above background?", Nicholson has

developed criteria for applying the Gaussian decision rule to test the significance of a difference between two Poisson distributions: the gross count C_{s+b} of sample plus background, measured over a time t_{s+b}, and the background count C_b, measured over a time t_b. For either C_{s+b} or C_b, the Poisson distribution can be written as

$$P(C;\mu) = \frac{\mu^C e^{-\mu}}{C!} , \qquad (1)$$

where μ is the mean of the distribution of observed counts C and $P(C;\mu)$ is the probability of observing C counts in a time t. Nicholson[5] has shown that for a desired level of confidence $100(1-\alpha)$ of less than or equal to 99% (i.e., for a value of α, the probability of incorrectly attributing nonzero net activity to the sample, of ≥ 0.01), the Gaussian approximation to the Poisson distribution is adequate when $(t_{s+b}/t_b)\mu_b \geq 50$ and $(t_{s+b}/t_b) \leq 1$. Using this approximation, he then presents a decision rule by which the hypothesis of nonzero sample activity can be tested in terms of the actual observable quantities C_{s+b}, C_b, t_{s+b} and t_b.

Currie has presented a more thorough examination of the concept of detectability of net activity, presenting an unambiguous definition of the "limit of detectability". It is formulated, however, in terms of the unobservable parameters μ_s and μ_b, the means of the net and background count distributions, respectively.

The present treatment may be thought of as an extended examination of the concept of detectability, but expressed in terms of observable quantities (designated by Latin symbols), clearly distinguished from unobservables (designated by Greek symbols).

Moreover, we extend the treatment to the question of whether or not the sample's net activity exceeds some predetermined limit. The results of this treatment are presented in the form of graphs and step-by-step prescriptions by which the experimenter can preselect counting times (or numbers of accumulated counts) in order to resolve either of the two questions posed above with a desired level of confidence.

In the present report, we present only a brief summary of the method together with the results for a 95% level of confidence. The complete treatment, together with graphical data for other choices of confidence level, will be published.

CASE I. DOES THE SAMPLE EXHIBIT A NET ACTIVITY ABOVE BACKGROUND?

The quantity sought in any counting experiment is ρ, the "true count rate" or the "true disintegration rate" if absolute counting is being done. The problem is to relate the measured counts C_{s+b} and C_b to ρ. To this end, we pose the null hypothesis "$\rho = 0$" and derive a decision rule by means of which it can be tested. The risk of false detection of activity, i.e., the probability that the hypothesis is rejected when it is really true, is designated α. (This is commonly referred to as a "Type I error".) We also define a quantity $\bar{Q}_d$, the mean probability of detection, a function of σ and μ, and hence of the observables C_{s+b} and C_b. This quantity is analogous to one which is used in the statistical interpretation of power spectra. In the

present context Q_d is the probability of detecting [illegible] activity, while $\bar{Q}_d$ is the best estimate of Q_d derived from the observed value of C_s. The two quantities α and $\bar{Q}_d$, representing the risks of false detection and non-detection, are inversely related. For a fixed counting time, that is for a given u, a decrease in the risk of false detection entails an increased risk of non-detection; a decrease in both requires an increase in the total counting time. Using the Gaussian approximation and integrating over the distribution by means of a Simpson numerical quadrature, we obtain $\bar{Q}_d$ as a function of the ratio of C_s to its standard deviation. Then, applying the criterion of Loevinger and Berman[7] for obtaining a given relative precision of C_s in a minimum amount of counting time $t_{s+b} + t_b$, we calculate and plot as a function of R, the ratio of gross to net counting rates, the total number of gross counts which the experimenter must accumulate in order to obtain a result with the desired probabilities α and $\bar{Q}_d$. Using these data, the decision rule of Nicholson[8] is then applied to determine whether, with the chosen degree of certainty, the sample is active. Figure C1 is a plot of the results for the most common choice of α ($\alpha = 0.05$), and various choices of $\bar{Q}_d$. The ratio R is determined from a preliminary measurement of approximately 300 counts each on the sample and on background.

Thus, to determine whether a sample exhibits a net activity above background:

(1) Choose a value of α, the desired maximum probability of falsely concluding that the sample is active when it

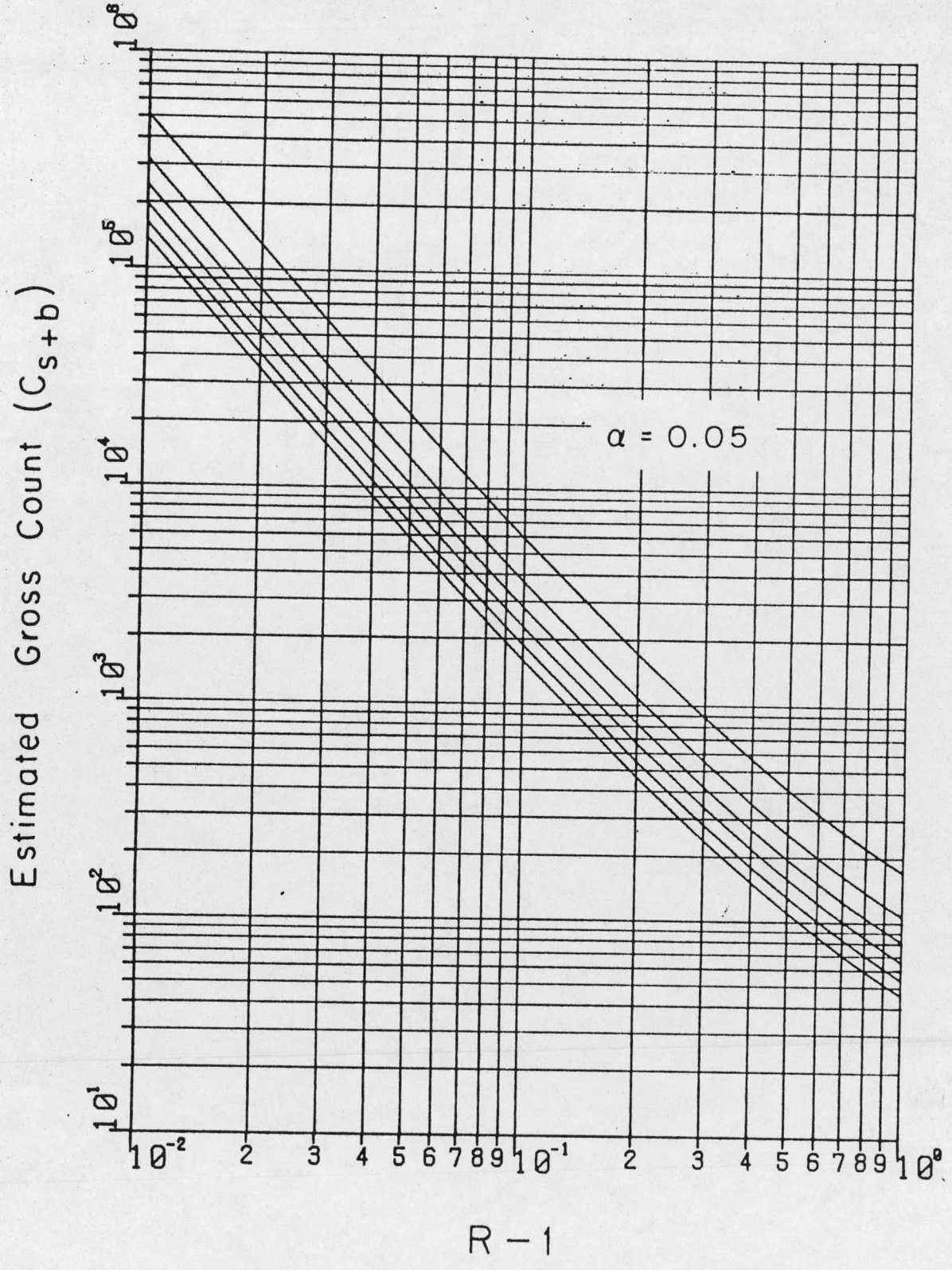

Fig. C1. Estimated gross count (C_{s+b}) which is necessary to achieve various mean probabilities of detection ($\overline{Q}_d$) for $\alpha = 0.05$, when testing a sample for nonzero net activity. R is the ratio of gross to background count rates from a preliminary measurement. Curves are for values of $\overline{Q}_d$ = 0.75, 0.80, 0.85, 0.90, 0.95, 0.99 (reading upward).

actually isn't. Choose also a value of β, the maximum acceptable risk of non-detection of activity. Then, $\bar{Q}_d$ is equal to $1-\beta$.

(2) Perform a preliminary measurement, of approximately 300 counts each, of the gross count C_{s+b} and the background count C_b. Record C_{s+b}, C_b, t_{s+b} and t_b.

(3) Calculate R from the equation

$$R = (C_{s+b}/t_{s+b}) / (C_b/t_b).$$

If R does not differ enough from unity to permit the use of Fig.C1, accumulate approximately 300 counts more for C_{s+b} and C_b and recalculate R from the combined (600-count) values.

(4) If the chosen value of α is 0.05, enter Fig.C1 to obtain an estimated value of the required number of gross counts C_{s+b}. (Curves for other values of α and $\bar{Q}_d$ will appear in the published work.) The corresponding number of background counts C_b is obtained from the relation

$$C_b = C_{s+b}/R^{3/2}.$$

(5) Accumulate counts until these values have been reached. Record C_{s+b}, C_b, t_{s+b} and t_b.

(6) Apply the following decision rule:

If the net sample count $\left(C_{s+b} - \frac{t_{s+b}}{t_b} C_b\right) > k_\alpha \left[C_{s+b} + \left(\frac{t_{s+b}}{t_b}\right)^2 C_b\right]^{\frac{1}{2}}$,

accept $\rho_{is} > 0$;

Otherwise, accept $\rho_s = 0$.

Some values of n_α to be used in this decision rule are:

$n_\alpha = 1.282$ for $\alpha = 0.10$, $n_\alpha = 1.645$ for $\alpha = 0.05$, and

$n_\alpha = 2.326$ for $\alpha = 0.01$.

Case II. IS THE ACTIVITY OF THE SAMPLE BELOW SOME PREDETERMINED LIMIT?

In this case, the hypothesis to be tested is that ρ_s exceeds some predetermined (safe) value ρ_c. The risk of incorrectly rejecting this hypothesis, i.e., of failing to note that the safe limit has been exceeded, is α. As in Case I, a mean power $\bar{Q}_d$ is formulated for the hypothesis test, the minimum-counting-time criterion of Loevinger and Berman is applied, and the equations are solved for the number of counts C_{s+b} necessary for the chosen values of α and $\bar{Q}_d$ as a function of observable parameters determined from a preliminary count. Figure C2 contains the results for $\alpha = 0.05$ and $\bar{Q}_d = 0.95$.

Thus, to determine whether a sample's net activity is below some predetermined value ρ_c:

(1) Choose a value of α, the desired maximum risk of failing to note that the sample's activity exceeds ρ_c. Choose also a value of β, the maximum acceptable risk of non-detection of activity. Then, $\bar{Q}_d$ is equal to $1-\beta$.

(2) Perform a preliminary measurement, of approximately 300 counts each, of the gross count C_{s+b} and the background count C_b. Record C_{s+b}, C_b, t_{s+b} and t_b.

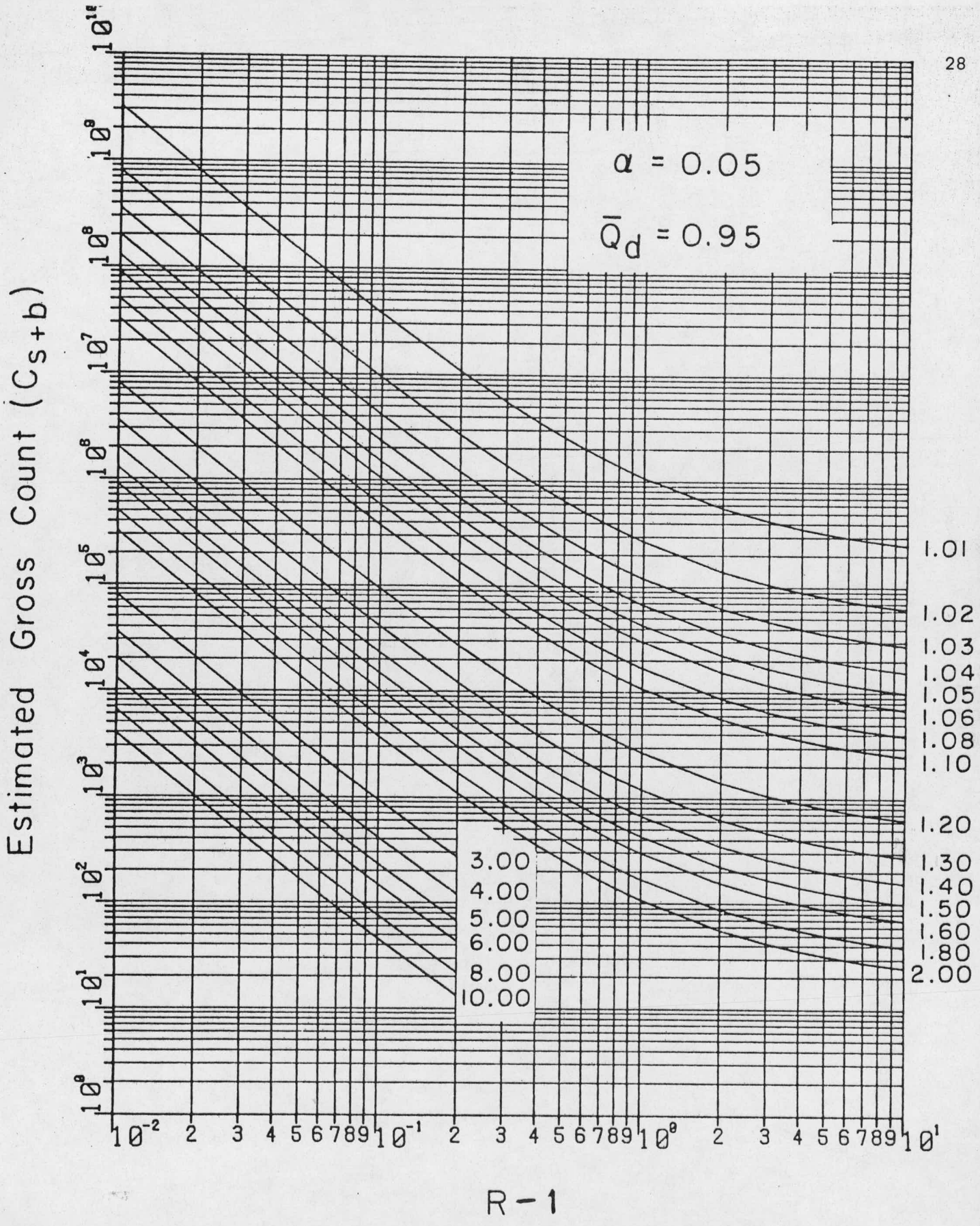

Fig. C2. Estimated gross count (C_{s+b}) which is necessary to achieve a specified mean probability of a correct decision regarding how ρ_s compares with a reference value ρ_c. The curves are labeled with their corresponding values of R_2. Values of R and R_2 are obtained from a preliminary measurement.

(3) Calculate R and R_2 from the following equations:

$$R = (C_{s+b}/t_{s+b}) / (C_b/t_b)$$

and

$$R_2 = \rho_c/(C_{s+b}/t_{s+b} - C_b/t_b).$$

If R and R_2 do not differ enough from unity to permit the use of Fig. C2, accumulate approximately 300 counts more for C_{s+b} and C_b and recalculate R and R_2 from the combined (600-count) values.

(4) If the chosen values of α and $\bar{Q}_d$ are 0.05 and 0.95, respectively, enter Fig. C2 to obtain an estimated value of the required number of gross counts C_{s+b}. (Curves for other values of α and $\bar{Q}_d$ will appear in the published work.) The corresponding number of background counts C_b is obtained from the relation

$$C_b = C_{s+b}/R^{3/2}.$$

(5) Accumulate counts until these values have been reached. Record C_{s+b}, C_b, t_{s+b} and t_b.

(6) Apply the following decision rule:

If the net sample count $\left|C_{s+b} - \frac{t_{s+b}}{t_b} C_b\right| < t_{s+b}\rho_c - n_\alpha\left[C_{s+b} + \left(\frac{t_{s+b}}{t_b}\right)^2 C_b\right]^{\frac{1}{2}}$,

Accept $\rho_s < \rho_c$;

Otherwise, accept $\rho_s \geq \rho_c$.

(Values of n_α to be used in this decision rule are the same as those given in the decision rule for Case I, above.)

The reference value ρ_c may be defined either in the same terms as ρ_s, e.g., as counts per minute on the same radiation

detector as is being used to count the sample, or as an absolute disintegration rate, e.g., in picocuries. In the latter case, the efficiency of the sample detector must be measured independently and the reference value ρ_c must be multiplied by this efficiency before being used in the decision rule given above.

D. Strontium and Radiostrontium in Marine Mollusc Shells

As indicated in our previous annual report, ^{90}Sr levels in marine bivalves from the Venezuelan coast are being measured in an attempt to establish baseline values for this radionuclide in the area. Our previous work was restricted in both method and number of samples; therefore, new techniques for the analysis of both ^{90}Sr and total Sr have been developed during the past year. These techniques were designed to be rapid, easily adaptable to the handling of a large number of samples in replicate analyses, and of the sensitivity and selectivity necessary for environmental samples.

For the determination of total strontium, atomic emission was chosen because it is sensitive, rapid and simple. Each shell sample is first cataloged and its physical properties recorded i.e., size, weight, shape), then calcined in a furnace at 500°C, pulverized, sampled and dissolved in concentrated HCl. The solution is filtered and then diluted to a known volume. Since a shell is a chemically complex material, the method of standard additions is used in order to eliminate any extraneous differences between the standards and the unknown samples. To use this method, the shell solution is divided into 5 equal-volume aliquots and to all but one of these, various known quantities of standard strontium solution are added. The relative emission intensity of each solution is determined by aspirating it into the flame of the atomic emission spectrometer, and the unknown concentration is then found by plotting emission intensity against amount of

added standard. This plot is a straight line, the equation for which is then ascertained by the linear least squares computer program SHELL to determine the abcissa intercept, which is the Sr concentration in the unknown solution.

Thus far, eighteen specimens of Lima scabra shells from a single location in Mochima Bay, Venezuela have been analyzed for total strontium. The results show substantial differences among individuals, ranging from 1.45 to 2.41 mg Sr/g ashed shell. Samples of other species are also being analyzed for total strontium. Then, ^{90}Sr analyses of all of these specimens are to be carried out, so that their ^{90}Sr content can be obtained as pCi ^{90}Sr/mg Sr = (pCi ^{90}Sr/g ashed shell) ÷ (mg Sr/g ashed shell).

The levels of ^{90}Sr activity in the shells are being determined by a newly-developed radiochemical separation procedure, in which the previously-employed strontium nitrate precipitation method is replaced by an extraction procedure for the yttrium-90 daughter. It has been reported [D.F.Peppard et al., J. Inorg. Nucl. Chem. 5, 141 (1957)] that a 1.5M solution of di-2-ethylhexyl phosphoric acid (known as HDEHP) in toluene preferentally extracts yttrium from 0.05M HCl solution with a concentration factor of yttium over strontium of some 2×10^6. Following indications in the literature that commercial HDEHP is a mixture of the mono and diesters and that only the diester is effective in extracting Y, a purification procedure appeared to be necessary. To determine the relative amounts of the two esters before and after the purification, an analytical procedure, involving potentiometric titration with NaOH in a methanol solvent medium, had to be developed. The titration procedure

was based on a series of experiments which showed that the end points of the two neutralizable hydrogens (one on the diester and two on the monoester) are well separated in methanol as a solvent.

The purification procedure adapted for crude HDEHP employs a seven-stage diamond extraction procedure, with the opposing phases comprising HDEHP in ether and ethylene glycol. The extraction can be understood by reference to Fig. D1, in which the circles represent separatory funnels and the arrows indicate the direction of solvent flow. The seven separatory funnels are placed on a rack and the extraction is begun by adding crude HDEHP, ether and ethylene glycol (in the ratio 4:7:1) to funnel No. 4, equilibrating, then transferring the ether layer into funnel No. 3 and the ethylene glycol layer in funnel No. 5. Fresh solvent is then added to these two funnels, and so on according to the diagram. All of the ether layers are combined and evaporated under reduced pressure until the ether is completely removed and only the HDEHP remains. This once-purified HDEHP can be put through the diamond extraction procedure again to yield twice-purified HDEHP.

The methanol potentiometric titration analyses showed that this purification procedure was indeed effective in removing monoester from the reagent. Crude, once-purified, and twice-purified HDEHP were then tested for ^{90}Sr - ^{90}Y separation efficiency by observing the beta spectra of ^{90}Sr and ^{90}Y in a liquid scintillation spectrometer both before and after purification. The results indicated that, contrary to indications in the literature, the crude and purified reagents were equally effective in separating Y from Sr. In

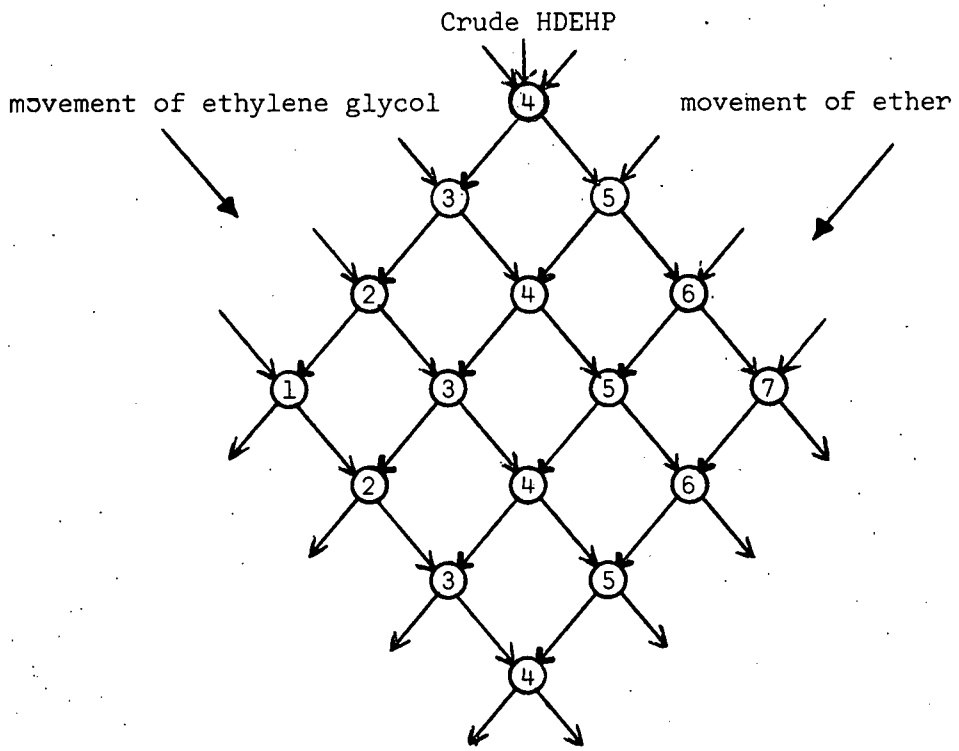

Figure D1. Multiple fractional distribution for the separation of HDEHP and H_2MEHP.

subsequent radiochemical separations, then, the commercial reagent is being used as received.

Strontium-90 analyses of the shell specimens are thus ready to be carried out, pending completion of our new low-level counting facility. (See Section E, below.)

E. New Counting Facilities

1. Electronics

During the past year all of the electronics in our eighth-floor counting room were replaced with modern solid-state equipment (not funded by the present contract). All of the research detectors are now equipped with NIM electronics which are interchangable and compatible with an automatic printing control unit. In addition, new gas flow controls have been installed for the two methane proportional flow counters and for the 4π proportional counter. These controls permit rapid, reproducible setting of the flow rates and accurate monitoring of gas flow through the counters.

2. Low-Level Counting

As noted in last year's report, our new chemistry building has a below-grade-level isotope storage facility containing a four-by-six by five-foot-deep concrete pit. Since the facility has to date remained unused for isotope storage, it is being converted into a low-level counting room, for which it appears to be ideally suited, since it is shielded above by fourteen stories of cast-in-place concrete building and on the five other sides by poured concrete footing. The walls and floor of the room and pit are coated with white glazed epoxy paint. An isolated, "quiet" instrument ground has been installed, provisions have been made for controlled personnel access, and a filtered ventilation system has been added.

The Beckman Low-level, anticoincidence-shielded, α and β counter has been stripped of its electronics and completely new NIM units have

been installed, together with newly-designed and constructed sample-changer logic electronics. The counter and sample-changer have been installed in the five-foot-deep pit while the electronics, which are now undergoing testing, have been installed at work-table level in the room. All of the NIM electronics in the low-level counter and all of these in the eighth-floor counting room are from the same manufacturer (ORTEC) and easily interchanged in case of malfunction. On completion of the use-testing of the new low-level electronics system, counting of the marine specimens will begin.

F. Other Facility Improvements

1. Negative Ion Source

Work has continued on the development of heavy ion beams from the Nuclear Physics Lab's Extrion Universal Negative Ion Source (UNIS). Usable beams of ^{58}Ni, ^{48}Ti, ^{12}C, ^{16}O and ^{32}S have been obtained thus far. During the past year, our group has been involved in the development of these beams, particularly of the ^{58}Ni and ^{48}Ti beams used in our charge-state work.

It has been observed that UNIS produces molecular ions in addition to monatomic ions. For ^{58}Ni, the predominant species emitted from the source is $^{58}Ni^-$, and this is the ion which is injected into the accelerator. For ^{48}Ti, however, TiO^- or TiO_2^- are the predominant species, and to obtain maximum beam intensity for purposes of accelerator stability, these are the ions which are chosen for injection. These molecular ions break apart when the beam passes through the accelerator's stripper foils, however, and $^{48}Ti^-$ is accelerated through the remainder of the machine.

2. Evaporator

Installation of the Varian NRC 3117 Vacuum Coater System was completed this year. The final components in the target preparation system consisted of a quartz crystal microbalance and a Hewlett-Packard 5381A, 80MHz frequency counter. With this new equipment, errors in thickness determination due to electronic instabilities should be less than 0.05 $\mu g/cm^2$. Calibration of this system with weighed foils is now in progress.

G. Computation

This year our use of the computer facility at the Nuclear Physics Laboratory (NPL) has increased drastically. All of the Ni and Ti charge-state data were collected with the PDP 15 computer on-line. Data acquisition was controlled by the NPL singles code SNAP. The data were stored on magnetic tapes, and could also be transferred directly to the off-line PDP 15. Preliminary data analysis, consisting of peak integration and background subtraction, was performed on this computer using the NPL code PEAK.

The heavy-ion fusion experiment entailed an extensive amount of computer programming. The major results of this work are a four-parameter data acquisition code, MAP.H, which is tailored to this particular experiment, and a rather general four-dimensional stripping code, WINDOW. Various testing and utility codes have also been developed to support this experiment.

Once again our use of the University of Pittsburgh's PDP 10 computer has been extensive. During the past year, a code was developed to perform all normalizations, data analysis and plotting for the charge-state experiment. All DWBA and kinematic calculations were also performed on this system. In addition, the Blann-Plasil code ALICE was adapted for use on the PDP 10.

All calculations necessary for the low-level counting statistics project were performed on the PDP 10, utilizing computer codes written in our laboratory. In addition, a computer program has been developed to permit rapid analysis of the total

strontium atomic emission data in the strontium-in-shell experiments. Finally, a non-linear least-squares program, far superior to our old code, was written this year.

III. PERSONNEL

Principal Investigator

Robert L. Wolke, Professor of Chemistry. B.S. Chem. Polytechnic Institute of Brooklyn 1949, Ph.D. Cornell University 1953. (Approximately one-third time January 1975 through April 1975, approximately one-third time May 1975 through December 1975.)

Other Research Personnel

Judith C. Brillhart, Graduate Research Assistant July 1974 - September 1974. B.S. Western Illinois University 1971. (Radioactivity in Mollusc Shells). Terminated June 1975.

Jack J. Donn, Captain, U.S. Air Force. Civilian Institutions Student, U.S. Air Force Institute of Technology (Not supported on ERDA contract funds.) B. S. University of Cincinnati 1968. (Statistics of Low-Level Counting). Terminated July 1975.

Martin E. Hughes, Research Assistant, full time. B.S. University of Pittsburgh 1975. (Strontium in Mollusc Shells).

William J. Jordan, Mellon Fellow. (Not supported on ERDA contract funds.) B.S. University of Pittsburgh 1973. (Heavy-Ion Reactions).

John D. Yesso, Graduate Research Assistant. B.S. University of Pittsburgh 1971. (Equilibrium Charge-State Distributions of Heavy Ions).

Other Personnel

Patricia Moan, Secretary. April 1974 to present.

Ronald E. Bajuscak, Undergraduate assistant. (Strontium and Radiostrontium Analysis)

Susan Wozniak, Undergraduate Assistant. (New Target Preparation Techniques)

IV. PUBLICATIONS

(Publications listed either have appeared in 1975, are in press, or have been submitted for publication.)

Spin Assignments in the Decay of Indium 109. S. Shastry, T. W. Debiak, E. V. Mason, Jr., J. D. Yesso and R. L. Wolke Particles and Nuclei, August 1975 (in press)

A Search for Alpha Instability in Osmium-184. Robert F. Sperlein and Robert L. Wolke, J. Inorg. Nucl Chem. 38, 27 (1975)

The Practical Design and Statistical Interpretation of Background-Dominant Counting Experiments, Jack J. Donn and Robert L. Wolke, Radiochem. and Radioanalyt. Lett. (submitted)

The Statistical Interpretation of Counting Data from Measurements of Low-Level Radioactivity. Jack J. Donn and Robert L. Wolke, Health Phys. (submitted)